SIAM J. SCI. COMPUT.
Vol. 41, No. 3, pp. A1753–A1776

THE CONJUGATE FUNCTION METHOD AND CONFORMAL MAPPINGS IN MULTIPLY CONNECTED DOMAINS*

HARRI HAKULA†, TRI QUACH†, AND ANTTI RASILA‡

Abstract. The conjugate function method is an algorithm for numerical computation of conformal mappings for simply and doubly connected domains. In this paper the conjugate function method is generalized for multiply connected domains. The key challenge addressed here is the construction of the conjugate domain and the associated conjugate problem. All variants of the method preserve the so-called reciprocal relation of the moduli. An implementation of the algorithm is given along with several examples and illustrations.

Key words. numerical conformal mappings, conformal modulus, multiply connected domains, canonical domains

AMS subject classifications. 30C30, 65E05, 31A15, 30C85

DOI. 10.1137/17M1124164

1. Introduction.

Conformal mappings play an important role in theoretical complex analysis and in certain engineering applications, such as electrostatics, aerodynamics, and fluid mechanics. Existence of conformal mappings of simply connected domains onto the upper half-plane or the unit disk follows from the Riemann mapping theorem, and there are generalizations of this result for doubly and multiply connected domains [2]. However, constructing such mappings analytically is usually very difficult, and numerical methods are required.

There exists an extensive literature on numerical construction of conformal mappings for simply and doubly connected domains [26]. One popular method is based on the Schwarz–Christoffel formula [13], and its implementation SC Toolbox is due to Driscoll [11, 12]. SC Toolbox itself is based on an earlier FORTRAN package by Trefethen [29]. A new algorithm involving a finite element method and the harmonic conjugate function was presented by the authors in [15].

While the study of numerical conformal mappings in multiply connected domains dates back to the 1980s [24, 27], recently there has been significant interest in the subject. DeLillo, Elcrat, and Pfaltzgraff [9] were the first to give a Schwarz–Christoffel formula for unbounded multiply connected domains. Their method relies on the Schwarzian reflection principle. Crowdy [4] was the first to derive a Schwarz–Christoffel formula for bounded multiply connected domains, which was based on the use of the Schottky–Klein prime function. In a very recent paper [28] conformal maps from multiply connected domains onto lemniscatic domains have been discussed. The natural extension of this result to unbounded multiply connected domains is given in [5]. It should be noted that a MATLAB implementation of the Schottky–Klein prime function is freely available [7], and the algorithm is described in [8]. A method involving the harmonic conjugate function is given in [23], but the approach there differs

*Submitted to the journal's Methods and Algorithms for Scientific Computing section April 4, 2017; accepted for publication (in revised form) February 21, 2019; published electronically May 23, 2019.

http://www.siam.org/journals/sisc/41-3/M112416.html

†Institute of Mathematics, Aalto University, FI-00076 Aalto, Finland (harri.hakula@aalto.fi, tri.quach@aalto.fi).

‡Guangdong Technion – Israel Institute of Technology, College of Science, Shantou, Guangdong 515063, China (antti.rasila@iki.fi, antti.rasila@gtiit.edu.cn).

from ours. Still another approach is given by Zeng and et al. [32], where Koebe's conventional method for multiply connected planar surfaces is generalized.

The foundation of conjugate function methods for simply and doubly connected domains lies on properties of the (conformal) modulus, which originates from the theory of quasiconformal mappings [1, 22, 26]. Here we investigate conformal mappings onto two types of canonical domains, and the associated boundary value problems that are, respectively, intended to generalize the concepts of the canonical quadrilateral and the ring domain, conformal mappings of which were investigated in [15]. In the following, for convenience we refer to these two classes of problems as Q-type and R-type, respectively.

Heuristically, the Q-type configuration refers to the situation where the ideal fluid flows from one arc on the exterior component of the boundary to another, and the interior components of the boundary are understood as nonabsorbing. In this case, the canonical domain is a rectangle where the width is normalized to be one, the height is a number $d > 0$ that can be understood as the modulus of the curve family connecting the above-mentioned boundary arcs, and the interior components of the boundary are mapped onto horizontal slits. The R-type configurations generalize the concept of the ring domain, where ideal fluid flows from interior boundary components to the exterior boundary. In this case, the canonical domain is the spherical annulus $A_{\log R} = \{z : 1 < |z| < R\}$ with radial slits. For simplicity, we investigate only the case of a Denjoy domain, where the canonical domain can be chosen so that the boundary components map onto line segments on the positive real axis. In particular, this is true for all triply connected domains (cf. [14, pp. 128–130]).

In terms of partial differential equations (PDEs), the conformal mapping is defined by a harmonic potential u and its harmonic conjugate v. One has to first find the potential u by solving the Laplace equation $\Delta u = 0$ in the domain Ω, with boundary conditions

$$\mathbb{1}_N \frac{\partial u}{\partial n} + \mathbb{1}_D u = f(x, y) \text{ on } \partial\Omega, \tag{1.1}$$

where the indicator functions refer to Neumann and Dirichlet boundary parts, respectively. These boundary conditions can be defined by the application, thus determining the type of the problem, or alternatively the choice of the preferred mapping determines the boundary conditions. In the cases considered here, from the solution u one can formulate a conjugate problem with a solution v, the harmonic conjugate of u, and together u and v define the conformal mapping. Crucially, when the conjugate problem is formulated, it is possible that cuts are introduced into the domain, and therefore the computational domain is not necessarily the same in both solution steps.

Our two classes of problems are not exhaustive; however, the fundamental ideas presented here can be applied to configurations not directly addressed by this paper. In Figure 1.1 two representative mappings of the same domain are constructed. In both cases the canonical domains are slit domains, first catalogued by Koebe [21].

Our method is suitable for a very general class of domains, allowing curved boundaries and even cusps. The implementation of the algorithm is based on the *hp*-finite element method (*hp*-FEM) described in [16], and in [17] it is generalized to cover unbounded domains. In [18], the method has been used to compute moduli of domains with strong singularities.

The accuracy of the method has been evaluated by solving three benchmark problems: one computing resistances [10] and two on capacities [3]. In each case the results agree with those obtained with either special-purpose methods or adaptive h-FEM.

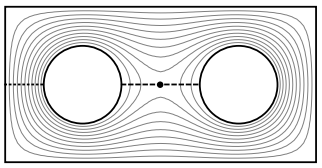

(a) R-type. Contour plot of u. Dirichlet on all boundaries. Interior $u = 1$, exterior $u = 0$. Saddle point and cuts are indicated.

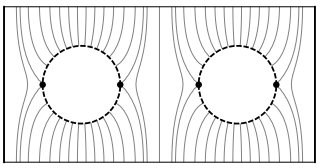

(b) Q-type. Contour plot of u. Dirichlet on left ($u = 0$) and right ($u = 1$). Neumann zero-condition on other boundaries. Locations of maxima and minima on the interior boundaries are indicated.

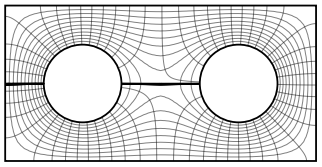

(c) R-type. Contour plot of u and v. Cuts are equipotential lines in v.

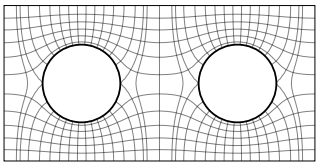

(d) Q-type. Contour plot of u and v.

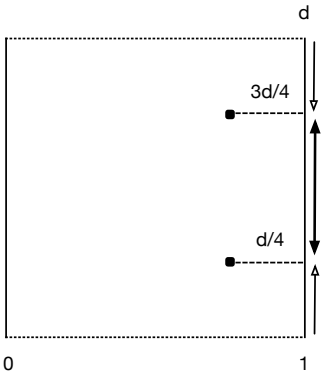

(e) R-type. Canonical domain in (u, v). Image scaled to $d = 1$. Saddle point lies on two oriented cuts. Width of the slit is determined by the potential of u at the saddle point. This domain can be further mapped to annulus A_d.

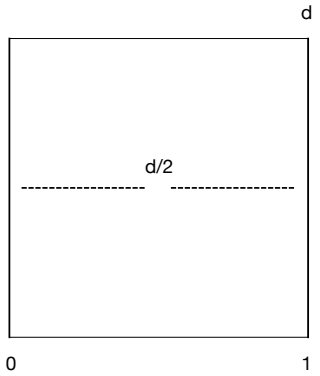

(f) Q-type. Canonical domain in (u, v). Image scaled to $d = 1$. Width of the slit is determined by the potential difference of u at the local maximum and minimum.

FIG. 1.1. *Conjugate function method and conformal mappings: Two circles in rectangle.*

The rest of the paper is organized as follows. In section 2 the necessary concepts from function theory are introduced. The new algorithms for multiply connected domains are described in sections 3 and 4 for types of R and Q, respectively. After the numerical implementation is discussed, an extensive set of numerical experiments is analyzed before brief conclusions are given.

2. Preliminaries. In this section we introduce concepts from function theory and review the algorithm for simply or doubly connected domains. For details and references, see [15].

DEFINITION 2.1 (modulus of a quadrilateral). *A Jordan domain Ω in $\mathbb{C}$ with marked (positively ordered) points $z_1, z_2, z_3, z_4 \in \partial\Omega$ is called a quadrilateral and denoted by $Q = (\Omega; z_1, z_2, z_3, z_4)$. Then there is a canonical conformal map of the quadrilateral Q onto a rectangle $R_d = (\Omega'; 1 + id, id, 0, 1)$, with the vertices corresponding to where the quantity d defines the modulus of a quadrilateral Q. We write*

$$\mathrm{M}(Q) = d.$$

Notice that the modulus d is unique.

LEMMA 2.2 (reciprocal identity). *The reciprocal identity*

$$\mathrm{M}(Q)\,\mathrm{M}(\tilde{Q}) = 1 \tag{2.1}$$

holds, where $\tilde{Q} = (\Omega; z_2, z_3, z_4, z_1)$ is called the conjugate quadrilateral of Q.

2.1. Dirichlet–Neumann problem. It is well known that one can express the modulus of a quadrilateral Q in terms of the solution of the Dirichlet–Neumann mixed boundary value problem.

Let Ω be a domain in the complex plane whose boundary $\partial\Omega$ consists of a finite number of piecewise regular Jordan curves, so that at every point, except possibly at finitely many points of the boundary, an exterior normal is defined. Let $\partial\Omega = A \cup B$, where both A, B are unions of regular Jordan arcs such that $A \cap B$ is finite. Let ψ_A, ψ_B be real-valued continuous functions defined on A, B, respectively. Find a function u satisfying the following conditions:

1. u is continuous and differentiable in $\overline{\Omega}$.
2. $u(t) = \psi_A(t)$ for all $t \in A$.
3. If $\partial/\partial n$ denotes differentiation in the direction of the exterior normal, then

$$\frac{\partial}{\partial n} u(t) = \psi_B(t) \quad \text{for all } t \in B.$$

The problem associated with the conjugate quadrilateral $\tilde{Q}$ is called the *conjugate Dirichlet–Neumann problem.*

Let $\gamma_j, j = 1, 2, 3, 4$, be the arcs of $\partial\Omega$ between (z_1, z_2), (z_2, z_3), (z_3, z_4), (z_4, z_1), respectively. Suppose that u is the (unique) harmonic solution of the Dirichlet–Neumann problem with mixed boundary values of u equal to 0 on γ_2 and to 1 on γ_4, and $\partial u/\partial n = 0$ on γ_1, γ_3. Then

$$\mathrm{M}(Q) = \iint_\Omega |\nabla u|^2 \, dx\, dy. \tag{2.2}$$

Suppose that Q is a quadrilateral and u is the harmonic solution of the Dirichlet–Neumann problem, and let v be a conjugate harmonic function of u, $v(\mathrm{Re}\, z_3, \mathrm{Im}\, z_3) = 0$. Then $f = u + iv$ is an analytic function, and it maps Ω onto a rectangle R_h such that the images of the points z_1, z_2, z_3, z_4 are $1 + id, id, 0, 1$, respectively. Furthermore, by Carathéodory's theorem, f has a continuous boundary extension which maps the boundary curves $\gamma_1, \gamma_2, \gamma_3, \gamma_4$ onto the line segments $\gamma_1', \gamma_2', \gamma_3', \gamma_4'$.

LEMMA 2.3. *Let Q be a quadrilateral with modulus d, and let u be the harmonic solution of the Dirichlet–Neumann problem. Suppose that v is the harmonic conjugate function of u, with $v(\mathrm{Re}\, z_3, \mathrm{Im}\, z_3) = 0$. If $\tilde{u}$ is the harmonic solution of the Dirichlet–Neumann problem associated with the conjugate quadrilateral $\tilde{Q}$, then $v = d\tilde{u}$.*

2.2. Ring domains. Let E_0 and E_1 be two disjoint and connected compact sets in the extended complex plane $\mathbb{C}_\infty = \mathbb{C} \cup \{\infty\}$. Then one of the sets E_0 or E_1 is bounded, and without loss of generality we may assume that it is E_1. Then a set $R = \mathbb{C}_\infty \backslash (E_0 \cup E_1)$ is connected and is called a *ring domain*. The *capacity* of R is defined by

$$\operatorname{cap}(R) = \inf_u \iint_R |\nabla u|^2 \, dx \, dy,$$

where the infimum is taken over all nonnegative, piecewise differentiable functions u with compact support in $R \cup E_0$ such that $u = 1$ on E_0 and $u = 0$ on E_1. Suppose that a function u is defined on R with 1 on E_0 and 0 on E_1. Then if u is harmonic, it is unique and minimizes the integral above. The conformal modulus of a ring domain R is defined by $\mathrm{M}(R) = 2\pi/\operatorname{cap}(R)$. The ring domain R can be mapped conformally onto the annulus A_r, where $r = \mathrm{M}(R)$.

2.3. Conjugate function method. For simply connected domains the conjugate function method can be defined in three steps.

ALGORITHM 2.4 (conjugate function method).

1. *Solve the Dirichlet–Neumann problem to obtain u and compute the modulus d.*
2. *Solve the Dirichlet–Neumann problem associated with $\tilde{Q}$ to obtain v.*
3. *Then $f = u + idv$ is the conformal mapping from Q onto R_d such that the vertices (z_1, z_2, z_3, z_4) are mapped onto the corners $(1 + id, id, 0, 1)$.*

For ring domains the algorithm has to be modified of course, and here the fundamental step is the cutting of the domain along the path of steepest descent, which enables us to return the problem to settings similar to those for the simply connected case.

ALGORITHM 2.5 (conjugate function method for ring domains).

1. *Solve the Dirichlet problem to obtain the potential function u and the modulus* $\mathrm{M}(R)$.
2. *Cut the ring domain through the steepest descent curve which is given by the gradient of the potential function u and obtain a quadrilateral where the Neumann condition is on the steepest descent curve and the Dirichlet boundaries remain as before.*
3. *Use the method for simply connected domains (Algorithm* 2.4*).*

Notice that the choice of the steepest descent curve is not unique due to the implicit orthogonality condition. In Figure 2.1 an example of the ring domain case is given. The key observation is that $d = \int_\Gamma |\nabla u| \, ds$, where Γ is any of the contour lines of the solution v. In Figure 2.1b the Dirichlet boundary conditions are set to be 0 and d instead of usual choices of 0 and 1. This choice does not have any effect on Figure 2.1c but is of paramount interest in the generalization of the algorithm.

DEFINITION 2.6 (cut). *A cut γ is a curve in the domain Ω, which introduces two boundary segments denoted by γ^+ and γ^- to the conjugate domain $\tilde{\Omega}$. Along the oriented boundary $\partial\tilde{\Omega}$, the segments γ^+ and γ^- are traversed in opposite directions.*

For the sake of discussion, below we define the conjugate problem directly. The cut γ (Definition 2.6) has its end points on ∂E_0 and ∂E_1. One choice for the (oriented) boundary of conjugate domain $\tilde{\Omega}$ starting from the end point of γ on ∂E_1 is given by the set $\{\gamma^+, \partial E_0, \gamma^-, \partial E_1\}$ as shown in Figure 2.1b. The boundary conditions are set as $u = 0$ on γ^+, $u = d$ on γ^-, and $\partial v/\partial n = 0$ on ∂E_j, $j = 1, 2$.

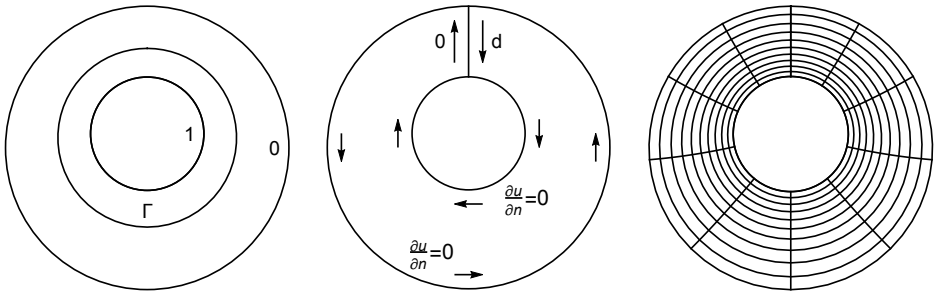

(a) Ring domain with boundary conditions. Γ is one of the contours, i.e., equipotential curves of the solution u.

(b) Conjugate domain $\tilde{\Omega}$ with boundary conditions. Here the Dirichlet boundary conditions are taken to be 0 and $d = \int_\Gamma |\nabla u| ds$.

(c) Conformal map. Contour lines of u and v.

FIG. 2.1. *Introduction to the conjugate function method for ring domains.*

2.4. Canonical domains. The so-called canonical domains play a crucial role in the theory of quasiconformal mappings (cf. [22]). These domains have a simple geometric structure. Let us consider a conformal mapping $f\colon \Omega \to D$, where D is a canonical domain and Ω is the domain of interest. The choice of the canonical domain depends on the connectivity of the domain Ω, and both domains D and Ω have the same connectivity. It should be noted that in simply and doubly connected cases, domains can be mapped conformally onto each other if and only if their moduli agree. In this sense, moduli divide domains into conformal equivalence classes. For simply connected domains, natural choices for canonical domains are the unit disk, the upper half-plane, and a rectangle. In the case of doubly connected domains an annulus is used as the canonical domain. For m-connected domains, $m > 2$, we have $3m - 6$ different moduli, which leads to various choices of canonical domains. These domains have been studied in [14, 25]. The generalization of the Riemann mapping theorem onto multiply connected domains is based on these moduli; see [14, Theorems 3.9.12 and 3.9.14].

3. Conjugate function method for multiply connected domains of type *R*. Let us first formally define the multiply connected domains of type R and their capacities. Let $m > 2$ and $E_0, E_1, \ldots, E_m$ be disjoint and nondegenerate continua in the extended complex plane $\mathbb{C}_\infty = \mathbb{C} \cup \{\infty\}$. Suppose that E_j, $j = 1, 2, \ldots, m$ are bounded; then a set $\Omega_{m+1} = \mathbb{C}_\infty \setminus \bigcup_{j=0}^m E_j$ is an $(m+1)$-connected domain, and its (conformal) capacity is defined by

$$\text{cap } (\Omega_{m+1}) = \inf_u \iint_{\Omega_{m+1}} |\nabla u|^2 \, dx \, dy,$$

where the infimum is taken over all nonnegative, piecewise differentiable functions u with compact support in $\bigcup_{j=1}^m E_j \cup \Omega_{m+1}$ such that $u = 1$ on E_j, $j = 1, 2, \ldots, m$ and 0 on E_0. Suppose that a function u is defined on Ω_{m+1} with 1 on E_j, $j = 1, 2, \ldots, m$ and 0 on E_0. Then if u is harmonic, it is unique, and it minimizes the integral above. The modulus of Ω_{m+1} is defined by $\text{M}(\Omega_{m+1}) = 2\pi/\text{cap } (\Omega_{m+1})$. If the degree of connectivity does not play an important role, the subscript will be omitted, and we simply write Ω.

In contrast with the ring problem there is no immediate way to define a conjugate problem. Indeed, it is clear that the conjugate domain *cannot* be a quadrilateral in the sense of the definitions above. However, there exists a contour line Γ_0 such that it encloses the sets $E_j,\ j = 1, 2, \ldots$, and

$$d = \mathrm{M}(\Omega_{m+1}) = \int_{\Gamma_0} |\nabla u|\, ds. \tag{3.1}$$

Thus, there is an analogue for the cutting of the domain along the curve of steepest descent. It can be assumed without loss of generality that the cut γ_0 (and the Dirichlet conditions) is/are between E_0 and E_1. Then the immediate question is how to cut the domain further between $E_j,\ j = 1, 2, \ldots, m$, in such a way that the conjugate domain is simply connected, and set the boundary conditions so that the Cauchy–Riemann equations are satisfied.

There is one additional property of the solution u that we can utilize. Namely, for every $E_j,\ j = 1, 2, \ldots$, there exists an enclosing contour line Γ_j. The capacity has a natural decomposition

$$d = \sum_j \hat{d}_j, \quad \hat{d}_j = \int_{\Gamma_j} |\nabla u|\, ds = \sum_k d_k = \sum_k \int_{\Gamma_{j,k}} |\nabla u|\, ds, \tag{3.2}$$

where $\Gamma_{j,k}$ denotes a segment from discretization of the contour line $\Gamma_j = \cup_k \Gamma_{j,k}$.

3.1. Saddle points. The saddle points of the solution u are of special interest. Notice that for simply and doubly connected domains they do not exist, and thus any generalization of Algorithm 2.4 must address them specifically. First, there are two steepest descent curves emanating from every saddle point. This means that in the conformal mapping of the domain, slits will emerge since the potential at the saddle point must be less than one. Second, analogously there are two steepest ascent curves reaching some boundary points z_i, z_j at boundaries ∂E_i, ∂E_j, respectively. In addition, we say that E_i and E_j are conformally visible to each other.

Remark. For symmetric configurations there may be more than two steepest descent and steepest ascent curves at the saddle point.

3.2. Cutting process. The orthogonality requirement implies that the curve formed by joining two curves of steepest descent from E_i and E_j meeting at the saddle point must be a contour line of the conjugate solution, that is, an equipotential curve. It follows that as in the doubly connected case, both boundary segments induced by a cut have a different Dirichlet condition. Therefore the cutting process can be outlined as follows.

ALGORITHM 3.1 (cutting process).

1. *Identify the saddle points* $s_k,\ k = 1, 2, \ldots$.
2. *Join the two curves of steepest descent from* ∂E_i *and* ∂E_j *meeting at the point* s_k *into cut* $\gamma_m,\ m \geq 1$.
3. *Starting from the first cut, form an oriented boundary of a simply connected domain by alternately traversing cuts* γ_m *and segments of* ∂E_j *induced by the cuts. Once the boundary is completed, every cut has been traversed twice (in opposite directions) and every* ∂E_j *has been traversed once.*

In Figure 3.1 two configurations are shown.

Remark. The symmetric case is covered if we allow for overlapping or partially overlapping cuts.

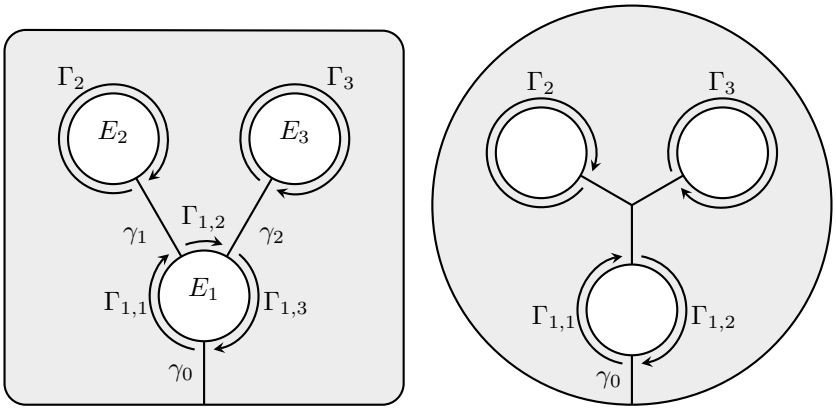

(a) Nonsymmetric case. Two saddle points, five jumps.

(b) Symmetric case. One saddle point, four jumps.

FIG. 3.1. *Examples of nonsymmetric and symmetric domains with cuts γ and decomposition of jumping curves $\Gamma_{i,k}$.*

3.3. Dirichlet conditions over cuts. Once the domain Ω has been cut and the oriented boundary of the conjugate domain $\tilde{\Omega}$ has been set up, it remains to set the Dirichlet conditions over the cuts. Given that the first cut leads to boundary conditions of 0 and d, it is sufficient to simply trace the oriented boundary of $\tilde{\Omega}$ and maintain the cumulative sum of jumps in modules computed over the segments $\Gamma_{j,k}$ connecting two consecutive cuts. Referring to Figure 3.1, notice that the identity (3.2) holds over the segments $\Gamma_{j,k}$.

ALGORITHM 3.2 (Dirichlet conditions over cuts).

1. *Set the Dirichlet boundary conditions of the boundary conditions induced by the first cut to* 0 *and* d.
2. *Trace the boundary starting from the zero boundary and update the cumulative sum of*
$$d_m = \int_{\Gamma_{j,k}} |\nabla u| \, ds,$$
where the $\Gamma_{j,k}$ are included in the order given by the boundary orientation.
3. *At every cut, set the Dirichlet condition to the cumulative sum reached at that point.*

3.4. Reciprocal identity. Suppose that u is the (unique) harmonic solution of the Dirichlet–Neumann problem given in the beginning of section 3. Let v be a conjugate harmonic function of u such that $v(\operatorname{Re}\tilde{z}, \operatorname{Im}\tilde{z}) = 0$, where $\tilde{z}$ is the intersection point of E_0 and γ_0^+.

Then $\varphi = u + iv$ is an analytic function, and it maps Ω onto a rectangle $R_d = \{z \in \mathbb{C} : 0 < \operatorname{Re} z < 1, 0 < \operatorname{Im} z < d\}$ minus $n-2$ line-segments, parallel to the real axis, between points $(u(\tilde{z}_j), d_j)$ and $(1, d_j)$, where $\tilde{z}_j$ is the saddle point of the corresponding jth jump. In the process we have a total of n jumps. See Figure 3.2 for an illustration of a triply connected example.

Let v be the harmonic solution satisfying the boundary values v equal to 0 on γ_0^+ and equal to 1 on γ_0^-, and Neumann conditions $\partial v/\partial n = 0$ on ∂E_j, $j = 0, 1, \ldots, m$. For the cutting curves γ_j, $j = 1, 2, \ldots, m$, we have Dirichlet conditions, and the value

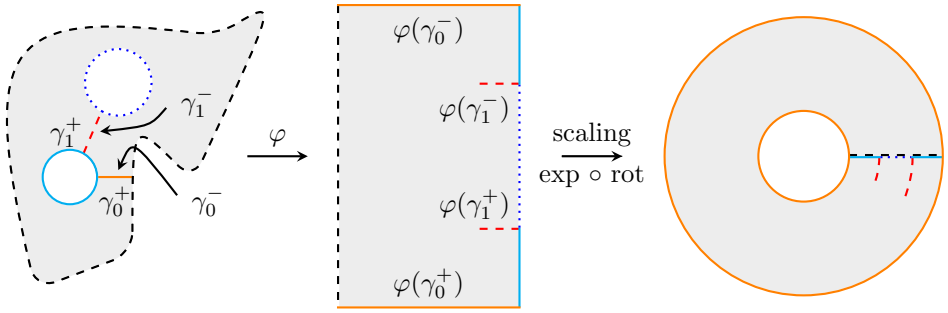

FIG. 3.2. *Construction of the conformal mapping from the domain of interest onto a canonical domain. In the first part, we use Algorithm* 3.5*, which creates the orange cut* γ_0 *and the dashed red cut* γ_1*. In the algorithm these cuts are traversed twice, which leads to two separated line-segments* $\varphi(\gamma_k^+)$ *and* $\varphi(\gamma_k^-)$ *on the rectangle. The latter part consist of a rotation, a scaling, and finally mapping with the exponential function. See online figure for color.*

is the cumulative sum $\sum_{j=0}^{m} d_j$. On the nth jump, we have on the corresponding cutting curve γ_j

$$v = \frac{\sum_{j=0}^{n} d_j}{d},$$

where d_j are given by (3.2). Note that if Γ_0 is an equipotential curve from γ_0^+ to γ_0^-, then we have

$$\mathrm{M}(\tilde{\Omega}) = \int_{\Gamma_0} |\nabla v|\, ds = \frac{1}{d}.$$

Thus we have the following proposition, which has the same nature as the reciprocal identity given in [16].

PROPOSITION 3.3 (reciprocal identity). *Suppose* u *and* v *are the solutions to problems on* Ω *and* $\tilde{\Omega}$*, respectively. If* $\mathrm{M}(\Omega)$ *denotes the integral of the absolute value of the gradient of* v *over the equipotential curve from* γ_0^+ *to* γ_0^-*, and* $\mathrm{M}(\tilde{\Omega})$ *denotes the same integral for* v*, then we have a normalized reciprocal identity*

$$\mathrm{M}(\Omega)\mathrm{M}(\tilde{\Omega}) = 1. \tag{3.3}$$

This reciprocal identity can be used in measuring the relative error of the conformal mapping. It should be noted that the mapping depends on $3m-6$ moduli. Thus, theoretically it is possible to have an incorrect result for some of the moduli such that the reciprocal identity holds. However, the probability of consistently having incorrect moduli for significant applications is extremely low.

LEMMA 3.4. *Let* Ω *be a multiply connected domain, and let* u *be the harmonic solution of the Dirichlet–Neumann problem. Suppose that* v *is the harmonic conjugate function of* u *such that* $v(Re\,\tilde{z}, Im\,\tilde{z}) = 0$*, where* $\tilde{z}$ *is the intersection point of* E_0 *and* γ_0^+*, and* d *is a real constant given by* (3.1)*. If* $\tilde{u}$ *is the harmonic solution of the Dirichlet–Neumann problem associated with the conjugate problem of* Ω*, then* $v = d\tilde{u}$*.*

Proof. It is clear that $v, \tilde{u}$ are harmonic. By the Cauchy–Riemann equations, we have $\langle \nabla u, \nabla v \rangle = 0$. We may assume that the gradient of u does not vanish on $\partial E_j, j = 0, 1, \ldots, m$. Then on ∂E_0, we have $n = -\nabla u/|\nabla u|$, where n denotes the exterior normal of the boundary. Likewise, we have $n = \nabla u/|\nabla u|$ on $\partial E_j, j =$

$1, 2, \ldots, m$. Therefore

$$\frac{\partial v}{\partial n} = \langle \nabla v, n \rangle = \pm \frac{1}{|\nabla u|} \langle \nabla v, \nabla u \rangle = 0.$$

On the cutting curves, from the Cauchy–Riemann equations we have that $|\nabla u| = |\nabla v|$, and from the jumping between cutting curves that $d = \sum_{j=0}^{n} d_j$. These results together imply that on the nth jump, we have on the corresponding cutting curve γ_k

$$v = \sum_{j=0}^{n} d_j.$$

Then by the uniqueness theorem for harmonic functions [2, p. 166], we conclude that $v = d\tilde{u}$.

Lastly, the proof of univalency of $\varphi = u + iv$ follows from the proof of univalency of f in [15, Lemma 2.3]. ∎

3.5. Outline of the algorithm. For convenience we use $\{\gamma\}$ and $\{\partial E\}$ to denote the sets of all cuts and boundaries, respectively.

ALGORITHM 3.5 (conjugate function method for multiply connected domains of type R).

1. *Solve the Dirichlet problem to obtain the potential function u and the modulus $d = \mathrm{M}(\Omega)$.*
2. *Choose one path of steepest descent reaching the outer boundary E_0, γ_0.*
3. *Identify the saddle points s_m.*
4. *For every saddle point: Find paths γ_k, $k > 1$, joining two conformally visible boundaries ∂E_i and ∂E_j by finding the paths of steepest descent meeting at the point s_m.*
5. *For every E_i: Choose a corresponding contour Γ_i, compute its subdivision $\Gamma_{i,k}$ induced by the paths $\{\gamma\}$, and the corresponding jumps $d_k = \int_{\Gamma_{i,k}} |\nabla u| ds$.*
6. *Construct the conjugate domain $\tilde{\Omega}$ by forming an oriented boundary using paths $\{\gamma\}$ and $\{\partial E\}$.*
7. *Set the boundary conditions along paths $\{\gamma\}$ by accumulating jumps in the order of traversal.*
8. *Solve the Dirichlet–Neumann problem on $\tilde{\Omega}$ for v.*
9. *Construct the conformal mapping $\varphi = u + idv$.*
10. *(Optional) Adjust the cuts and repeat the construction for the conjugate domain $\tilde{\Omega}$.*

3.6. Moduli and degrees of freedom. For $m+1$ connected domains, we have $3m-3$ different moduli, or degrees of freedom. In general, we have $2m-1$ jumps and $m-1$ saddle points. This sums up to $3m-2$. However, the cut γ_0 can be chosen so that the first and last jumps, d_1 and d_{2m-1}, respectively, are equal. Thus the number of degrees of freedom is reduced by one, and we obtain $3m-3$.

4. Conjugate function method for multiply connected domains of type *Q*. Let us next focus on the quadrilateral-like case, i.e., type Q. Conceptually the construction is much simpler than that of type R. Let the exterior boundary ∂E_0 be composed of four arcs ζ_i, $i = 1, 2, 3, 4$, in the sense of section 2.1, and the interior boundaries ∂E_j, $j = 1, \ldots, m$, have Neumann boundary conditions $\partial u / \partial n = 0$. Intuitively it is clear that the definition of the conjugate problem has to involve a

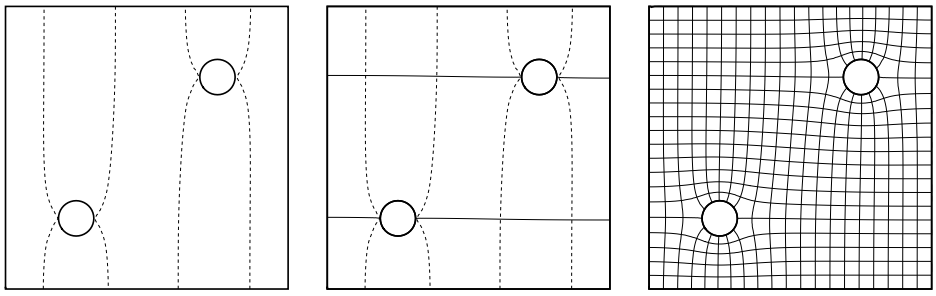

(a) Local maxima and minima of the interior boundaries. Equipotential curves.

(b) Geometric setting of potentials. Curves of steepest descent and ascent ρ_m.

(c) Map.

FIG. 4.1. *Q-type. Dirichlet conditions for the conjugate problem. Initially, conditions along the left-hand edge are* $u = 0$ *and along the right-hand edge are* $u = 1$.

Dirichlet–Neumann map and that there is no need for any cutting process. Once the potentials over ∂E_j, $j = 1, \ldots, m$, have been defined for the conjugate problem, the reciprocal identity follows immediately.

4.1. Dirichlet conditions over interior boundaries. Let us consider the configuration of Figure 4.1. In the initial problem the Dirichlet boundary conditions are $u = 0$ and $u = 1$ along the left- and right-hand edges (or ζ_1 and ζ_3, say), respectively. On every interior boundary ∂E_j, $j = 1, \ldots, m$, there are exactly two points with unique potentials that correspond to local maxima and minima, Figure 4.1a. Let us consider ∂E_j and denote the point with maximum potential x. Point x is connected with a point s on either one of the Dirichlet boundaries via a curve of steepest ascent ρ, Figure 4.1b. In the conjugate problem, the Dirichlet boundaries become Neumann. Along the Neumann edges the solution will be linear and have all values in the interval $[0, 1]$. Thus, the potential at the point s, and by construction at x since ρ is an equipotential curve in the conjugate problem, can be found using simple interpolation. The same procedure can be applied to the point of local minimum on ∂E_j. The resulting map is given in Figure 4.1c. If the potentials obtained by the interpolation procedure are not exact, they can be improved by constrained minimization of the reciprocal error $|1 - \mathrm{M}(\Omega)\mathrm{M}(\tilde{\Omega})|$. We have used the interior point method as implemented in Mathematica. This is computationally efficient, since only the right-hand sides of the linear systems are modified during optimization.

4.2. Outline of the algorithm. Let us assume that in the initial Dirichlet–Neumann problem, along the boundary segment ζ_1 the Dirichlet boundary condition is $u = 0$, and along ζ_3 is $u = 1$.

ALGORITHM 4.1 (conjugate function method for multiply connected domains of type Q).

1. *Solve the Dirichlet–Neumann problem to obtain the potential function* u *and the modulus* $d = \mathrm{M}(\Omega)$.
2. *Locate the local maxima and minima on the interior boundaries* ∂E_j, $j = 1, \ldots, m$.
3. *For every local maximum* x_m*: Find paths of steepest descent* ρ_m, $m > 1$, *connecting* x_m *on* ∂E_i *with the point* s_m *on* ζ_1. *(Or, for every local mimima* x_m*: Find paths of steepest ascent* ρ_m, $m > 1$, *connecting* x_m *on* ∂E_i *with the point* s_m *on* ζ_3.*)*

4. *Interpolate the potential on s_m on ζ_1 when ζ_1 is interpreted as a Neumann edge of the conjugate problem. (Or, similarly on ζ_3.)*
5. *Construct the conjugate domain $\tilde{\Omega}$ by performing the Dirichlet–Neumann map on ∂E_0 and setting the Dirichlet boundary conditions on ∂E_j, $j = 1, \dots, m$, to values obtained in the previous step.*
6. *Solve the Dirichlet–Neumann problem on $\tilde{\Omega}$ for v.*
7. *Construct the conformal mapping $\varphi = u + idv$.*
8. *(Optional) Improve the conjugate domain $\tilde{\Omega}$ by refining the Dirichlet boundary conditions via constrained minimization of the reciprocal error $|1-\mathrm{M}(\Omega)\mathrm{M}(\tilde{\Omega})|$.*

5. Numerical implementation of the algorithms. We use the implementation of the *hp*-FEM method described in detail in [16]. The strategy for computing the equipotential lines from the canonical domain onto the domain of interest can be found in [15].

The main difference between the two algorithms lies in the cuts between the sets E_j, $j = 1, 2, \dots, m$, in the case of type R, especially when locating the saddle point between sets. We use the Mathematica built-in constrained optimizer to locate the saddle points [31]. To find the actual cutting curve, we bisect ∂E_j, $j = 1, \dots, m$, and move against the gradient of u. By doing so, we search for a point on ∂E_j such that we end up within a tolerance from the saddle point.

If the cut can be computed analytically, the cut line can be embedded in the a priori mesh, and thus the same mesh can be used in both problems. In this situation it is sufficient to perform elemental integration once. The common blocks in the assembled linear systems can be eliminated as in [15, section 4.2]. In the general case, where the cutting has to be computed numerically, the meshes may vary over large regions, and the positive bias from reusing the mesh is lost.

For the Q-type, a similar iteration can be used to refine the potential values. In this case it may be necessary to refine the geometric search for the potential values.

Our algorithms involve computations that are not usually provided by standard FEM solvers. This is reflected in the relative computation times of the different parts of the algorithms. The relative maturity and level of implementation vary a lot over the solution process. In particular constrained triangulation with possibly large curved edges is not available in robust form and in path finding; for instance, in determining the cuts, the current data structures are not optimal.

6. Numerical experiments. In this section we discuss a series of benchmark problems and experiments carefully designed to illustrate different aspects of the algorithms. In electrostatics the Q-type refers to resistor design problems with multiple voltage domains, and the R-type refers to capacitor (electrical condenser) design domains. In practice, designing integrated circuits for multiple voltage domains is labor intensive, and there is a need for advanced design systems [20]. We have selected problems of both types from the literature and designed the experiments for the R-type. With two exceptions the examples involve multiply connected polycircular-arc domains. For an alternative solution method for this class of domains, see [6].

The use of the reciprocal relation as an error measure is formalized in the following definition.

DEFINITION 6.1 (reciprocal error). *Using Proposition* 3.3 *we can define two versions of the reciprocal error. First, for nonnormalized jumps,*

$$e_r^d = |1 - \mathrm{M}(\Omega)/\mathrm{M}(\tilde{\Omega})|, \tag{6.1}$$

and second, for the normalized jumps,

$$e_r^n = |1 - \mathrm{M}(\Omega)\mathrm{M}(\tilde{\Omega})|. \tag{6.2}$$

For convenience we define an associated error order.

DEFINITION 6.2 (error order). *Given a reciprocal error $e_r^\star$, the positive integer e_i,*

$$e_i = |\lceil \log(e_r^\star) \rceil|, \tag{6.3}$$

is referred to as the error order.

For the general case of R-type, the use of reciprocal error is not straightforward. The cuts must be approximated numerically, and the related approximation error leads to inevitable *consistency error* since the jumps depend on the chosen cuts. Thus, in order to have confidence in the general case as we do for the symmetric cases, one should consider a sequence of approximations for the cuts. Here, however, we are content to show via the conformal map that the chosen cut is a reasonable one, and the resulting map has the desired characteristics. For the Q-type consistency, error arises from locating the minima and maxima on the interior boundaries and subsequent determination of the Dirichlet data for the conjugate problems.

Of course, the exact potential functions are not known in general. However, we can always compute contour plots of the quantities of interest, that is, the absolute values of the derivatives, and get a qualitative idea of the overall performance of the algorithm. Naturally, this also measures the pointwise convergence of the Cauchy–Riemann problem.

One of the advantages of p- and hp-FEM is that exponential convergence in capacity can be achieved even in the case of singularities on the boundary if the mesh is graded geometrically. In our implementation the mesh refinement is done via recursive replacement rules in exact arithmetic, allowing for infinitesimal elements [19]. This allows us to generate nearly optimal a priori meshes followed by p refinement.

Data on benchmarks and basic experiments, including representative numbers for degrees of freedom assuming constant $p = 12$, is given in Tables 6.1 and 6.2b, respectively. In all cases the setup of the geometry is the most expensive part in terms of human effort and time. As usual in p- and hp-FEM, the computational cost in these relatively small systems is in integration and handling of the sparse systems. The actual computation times over the set of examples vary from seconds to minutes on standard desktop hardware using our implementation of the algorithms (Apple Mac Pro 2009 Edition 2.26 GHz, Mathematica 11.3).

6.1. Benchmarks. In [30] Trefethen gives an excellent introduction to the connection between conformal maps and computation of resistances of idealized planar resistors. In our setting the quantity of interest, the resistance of the resistor, is equal to the modulus of the conjugate domain. It should be mentioned that these benchmarks could be solved analytically using techniques described in [4].

6.1.1. Computation of resistances for quadrilaterals. Our first benchmark is of type Q (see Figure 6.1), a resistor first computed in [10]. The domain is enclosed by $B = [-3/2, 3/2] \times [-3/4, 3/4]$. There are two square holes (rotated by $\pi/4$),

$$H_1 = \{(-1/2, 0), (-3/4, 1/5), (-1, 0), (-3/4, -1/5)\},$$
$$H_2 = \{(1/2, 0), (3/4, -1/5), (1, 0), (3/4, 1/5)\},$$

TABLE 6.1
Data on benchmarks.

(a) Computed resistance.

Experiment	Capacity	Error order	(Reference)
Resistor	2.841998463680	11	(2.8419984)

(b) Computed capacity. (Error) refers to the reported estimated error of the reference.

Experiment	Capacity	(Reference)	(Error)
Capacitor A	9.49308124	(9.4930811)	(4e-7)
Capacitor B	8.47016014	(8.4701600)	(5e-7)

(c) FEM-data. Mesh (nodes, edges, triangles, quads). Degrees of freedom given at $p = 12$.

Experiment	Mesh	DOF
Resistor	(667,1236,16,552)	81935
Capacitor A	(509,946,8,428)	63143
Capacitor B	(1013,1910,0,896)	130439

TABLE 6.2
R-type. Data on experiments.

(a) Computed capacities.

Experiment	Capacity	Error order
Three disks in circle	9.67475429123	12
Two disks in rectangle	13.922976299110	12
Disk and Pacman in rectangle	13.3376294414	11

(b) FEM-data. Mesh (nodes, edges, triangles, quads). Degrees of freedom given at $p = 12$.

Experiment	Mesh	DOF
Three disks in circle	(35, 52, 0, 18)	2785
Two disks in rectangle	(34,49,0,16)	2509
Disk and Pacman in rectangle	(181,320,4,136)	20377

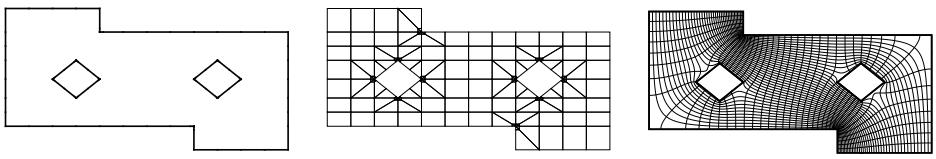

(a) Domain. (b) Mesh. (c) Map.

FIG. 6.1. *Resistor.*

and indentations

$$I_1 = [-3/2, 1/2] \times [-3/4, -1/2], \quad I_2 = [-1/2, 3/2] \times [1/2, 3/4].$$

The domain $\Omega = B \setminus (H_1 \cup H_2 \cup I_1 \cup I_2)$, with $\zeta_1 =$ along $y = 3/4$, $\zeta_3 =$ along $y = -3/4$, $\zeta_2 =$ path from $(-3/2, 3/4)$ to $(1/2, -3/4)$, and $\zeta_4 =$ path from $(3/2, -3/4)$

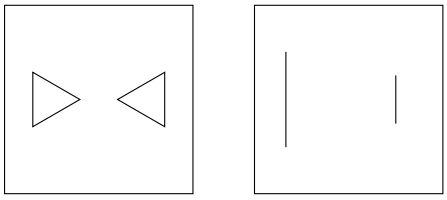

(a) Capacitor A. (b) Capacitor B.

FIG. 6.2. *Capacitors.*

to $(-1/2, 3/4)$. Formally the problems can be stated as

(6.4)
$$\begin{cases} \Delta u = 0 & \text{in } \Omega, \\ u = 0 & \text{on } \zeta_1, \\ u = 1 & \text{on } \zeta_3, \end{cases} \quad \text{leading to} \quad \begin{cases} \Delta v = 0 & \text{in } \tilde{\Omega}, \\ v = 1 & \text{on } \zeta_2, \quad v = 0.712841455, \quad \text{on } H_1, \\ v = 0 & \text{on } \zeta_4, \quad v = 0.287158545, \quad \text{on } H_2. \end{cases}$$

The computed value of resistance $\text{cap}(\tilde{\Omega}) = 2.841998463680$ is equal to that reported in [10]. Here we have adopted a convention used throughout in the experiments that Neumann zero boundary conditions are not defined separately but are implied unless otherwise specified.

6.1.2. Computation of capacities. We consider two cases, Capacitors A and B, Examples 7 and 10 from [3], respectively (see Figure 6.2). We compute only the capacities and do not treat these benchmarks as belonging to type R. In both cases the domain Ω is enclosed within $D = [-1, 1] \times [-1, 1]$. For Capacitor A, the plates are defined as the union of an equilateral triangle T and its reflection T' in the real axis. The vertices of T are the points $(a, 0)$, $(b, b - a)/\sqrt{3})$, and $(b, -(b - a)/\sqrt{3})$, where $0 < a < b < 1$. For Capacitor B, the plates are two slits $\overline{A_s B_s}$ and $\overline{C_s D_s}$, defined by points $A_s = (-2/3, -1/2)$, $B_s = (-2/3, 1/2)$, $C_s = (1/2, -1/4)$, $D_s = (1/2, 1/4)$. The computational domains are $\Omega_A = D \setminus (T \cup T')$ and $\Omega_B = D \setminus (\overline{A_s B_s} \cup \overline{C_s D_s})$. Thus, the corresponding problems are

$$(6.5) \quad \text{(A)} \begin{cases} \Delta u = 0 & \text{in } \Omega_A, \\ u = 0 & \text{on } \partial D, \\ u = 1 & \text{on } \partial T \text{ and } \partial T', \end{cases} \qquad \text{(B)} \begin{cases} \Delta u = 0 & \text{in } \Omega_B, \\ u = 0 & \text{on } \partial D, \\ u = 1 & \text{on } \overline{A_s B_s} \text{ and } \overline{C_s D_s}. \end{cases}$$

Choosing $a = 1/5$ and $b = 7/10$, we see that the computed capacity $\text{cap}(A) = 9.49308124$ is within the estimated error of the reference value. The computed capacity $\text{cap}(B) = 8.47016014$ is also within the estimated error of the reference value.

6.2. Symmetric case: Three disks in a circle. Consider a unit circle D_0 with three disks D_i, $i = 1, 2, 3$, of radius $r = 1/6$ placed symmetrically so that their origins lie on a circle of radius $r = 1/2$. We set $\Omega = D_0 \setminus (\cup_{i=1}^{3} D_i)$, and $\tilde{\Omega}$ contains five oriented cuts γ_k enumerated in the order of disks, starting from the outer circle

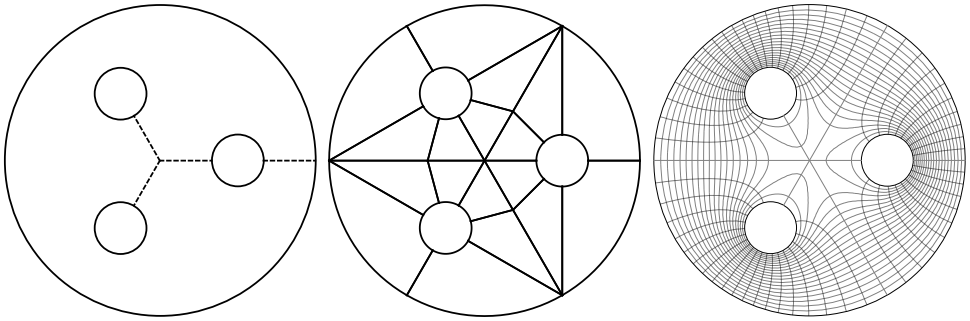

(a) Domain. (b) Mesh. (c) Map.

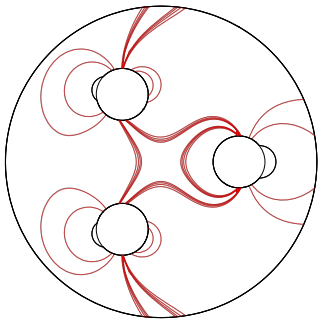

(d) Cauchy–Riemann. Contour lines of $|\partial u/\partial x|$ and $|\partial v/\partial y|$.

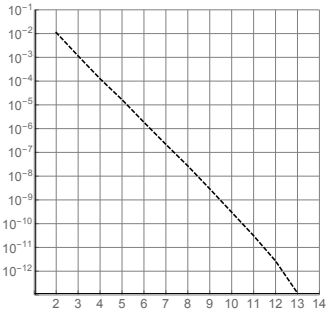

(e) Reciprocal identity. Convergence in p; log-plot, error versus p.

FIG. 6.3. *R-type. Fully symmetric case.*

D_0, $D_0D_1D_2D_3D_1D_0$. Using symmetry for the jumps, the problems can be written as

(6.6)

$$\begin{cases} \Delta u = 0 \text{ in } \Omega, \\ u = 0 \text{ on } \partial D_0, \\ u = 1 \text{ on } \cup_{i=1}^{3} \partial D_i, \end{cases} \quad \text{leading to} \quad \begin{cases} \Delta v = 0 \text{ in } \tilde{\Omega}, \\ v = 0 \text{ on } \gamma_1, \\ v = R/6 + (k-2)R/3 \text{ on } \gamma_k, \ k = 2,3,4, \\ v = R = 9.67475429123 \text{ on } \gamma_5. \end{cases}$$

As indicated in Figure 6.3a the cut can be computed analytically. The blending function approach used to compute higher order curved elements is very accurate if the element edges meet the curved edges at right angles. This is the reason for the mesh in Figure 6.3b where all edges adjacent to disks have been set optimally.

Notice that due to symmetry, the scaled jumps could also be computed analytically. However, in the numerical experiments, only computed values of Table 6.2a are used. Since the cuts are embedded in the mesh lines, both problems (the original and the conjugate) can be solved using the same mesh. In this optimal configuration, convergence in reciprocal relation is exponential in p, which is a remarkable result; see Figure 6.3e. Similarly, in Figure 6.3d, it is clear that the derivatives also have converged over the whole domain.

6.3. Axisymmetric cases. In the next three cases we maintain axial symmetry and thus analytic cuts. In the first two cases the enclosing rectangle $R = [-1,3] \times [-1,1]$, and in the third case $R_P = [-2,1] \times [-1,1]$.

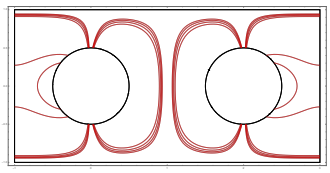

(a) Cauchy–Riemann. Contour lines of $|\partial u/\partial x|$ and $|\partial v/\partial y|$.

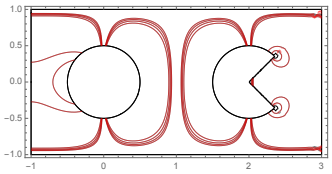

(b) Cauchy–Riemann. Contour lines of $|\partial u/\partial x|$ and $|\partial v/\partial y|$.

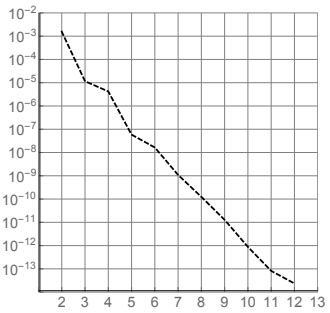

(c) Two disks in rectangle. Reciprocal identity. Convergence in p; log-plot, error versus p.

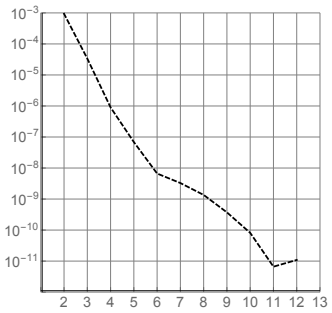

(d) Disk and Pacman in rectangle. Reciprocal identity. Convergence in p; log-plot, error versus p.

FIG. 6.4. *R-type. Axially symmetric cases.*

6.3.1. Two disks in a rectangle. Consider two disks D_1 and D_2 of radius $= 1/2$ with centers at $(0,0)$ and $(2,0)$, respectively. Here $\Omega = R \setminus (\cup_{i=1}^{2} D_i)$ and $\tilde{\Omega}$ contains four oriented cuts γ_k enumerated in the order of regions starting from R, $RD_1D_2D_1R$, and the problems can be stated as

(6.7)
$$\begin{cases} \Delta u = 0 \text{ in } \Omega, \\ u = 0 \text{ on } \partial R, \\ u = 1 \text{ on } \cup_{i=1}^{2} \partial D_i, \end{cases} \quad \text{leading to} \quad \begin{cases} \Delta v = 0 \text{ in } \tilde{\Omega}, \\ v = 0 \text{ on } \gamma_1, \\ v = M/4 + (k-2)M/2 \text{ on } \gamma_k, \ k = 2, 3, \\ v = M = 13.922976299110 \text{ on } \gamma_4. \end{cases}$$

The scaled jumps can be computed analytically, of course. The location of the saddle point is $x_s = (1, 0)$ and the corresponding value of $u(x_s) = 0.747496$. Once again, the reciprocal convergence in p is exponential (see Figure 6.4c). Similarly, the derivatives show convergence (see Figure 6.4a).

6.3.2. Disk and Pacman in rectangle. Next, the disk D_2 above is replaced by a disk with one quarter cut, C_1, the so-called Pacman. Now $\Omega = R \setminus (D_1 \cup C_1)$, and $\tilde{\Omega}$ contains four oriented cuts γ_k enumerated in the order of regions starting from R, $RD_1C_1D_1R$,

(6.8)
$$\begin{cases} \Delta u = 0 \text{ in } \Omega, \\ u = 0 \text{ on } \partial R, \\ u = 1 \text{ on } \partial D_1 \cup \partial C_1, \end{cases} \quad \text{leading to} \quad \begin{cases} \Delta v = 0 \text{ in } \tilde{\Omega}, \\ v = 0 \text{ on } \gamma_1, \\ v = \sum_{j=1}^{k-1} d_j \text{ on } \gamma_k, \ k = 2, 3, 4. \end{cases}$$

In this case we intentionally break the symmetry between meshes for the two

problems. The geometric refinement at the re-entrant corners is done in slightly different ways. The reciprocal convergence in p is exponential but with different rates at lower and higher values of p. Also, the difference in the number of refinement levels leads to a mild consistency error which appears as a loss of further convergence and accuracy at high p (see Figure 6.4d).

Here the jumps must be computed numerically (and tested against the computed capacity). Jumps have four decimals,

$$d_1 = 3.4808, d_2 = 6.3761, d_3 = 3.4808,$$

with $\mathrm{cap}(\Omega) = 13.3376294414$. The location of the saddle point is $x_s = (1, 0)$, and the corresponding value of $u(x_s) = 0.747475$, which does differ from the value observed for two circles. Again, the derivatives show convergence despite the re-entrant corners (see Figure 6.4b).

6.3.3. Pacman and droplet: Domain with cusp. Now the interior regions are a Pacman C at $(0, 0)$, and a domain B bounded by a Bezier curve,

$$\mathbf{r}(t) = \frac{1}{640}\left(45t^6 + 75t^4 - 525t^2 + 469\right) + \frac{15}{32}t\left(t^2 - 1\right)^2,\ t \in [-1, 1].$$

Let us first consider a corresponding problem of R-type. Let $\Omega = R_P \setminus (C \cup B)$, and $\tilde{\Omega}$ contains four oriented cuts γ_i enumerated in the order of regions starting from R_P, $R_P C B C R_P$,

$$\text{(6.9)} \qquad \begin{cases} \Delta u = 0 \text{ in } \Omega, \\ u = 0 \text{ on } \partial D_0, \\ u = 1 \text{ on } \partial D_{1,2,3}, \end{cases} \quad \text{leading to} \quad \begin{cases} \Delta v = 0 \text{ in } \tilde{\Omega}, \\ v = 0 \text{ on } \gamma_1, \\ v = \sum_{j=1}^{k-1} d_j \text{ on } \gamma_k,\ k = 2, 3, 4. \end{cases}$$

In [15] a ring domain with the same curve was considered up to very high accuracy. Notice that the "droplet" is designed so that also the tangents are aligned for parameter values $t = \pm 1$, and thus the opening angle is 2π requiring strong grading of the mesh. The resulting map is shown in Figure 6.5d. Letting $p = 16$ and using 14 levels of refinement at the three singularities, we see that the computed jumps are

$$d_1 = 3.3449, d_2 = 4.08337, d_3 = 3.3449,$$

with $\mathrm{cap}(\Omega) = 10.7732$. The location of the saddle point is $x_s = (-0.199, 0)$, and the corresponding value of $u(x_s) = 0.7540$. The error order $= 6$.

Next we set up a corresponding problem of Q-type as follows: $\zeta_1 =$ along $x = -1$, $\zeta_2 =$ along $y = -1$, $\zeta_3 =$ along $x = 3$, $\zeta_4 =$ along $y = 1$,

$$\text{(6.10)} \qquad \begin{cases} \Delta u = 0 & \text{in } \Omega, \\ u = 0 & \text{on } \zeta_1, \\ u = 1 & \text{on } \zeta_3, \end{cases} \quad \text{leading to} \quad \begin{cases} \Delta v = 0 & \text{in } \tilde{\Omega}, \\ v = 0 & \text{on } \zeta_2, \quad v = 1/2, \quad \text{on } C, \\ v = 1 & \text{on } \zeta_4, \quad v = 1/2, \quad \text{on } B. \end{cases}$$

Again letting $p = 16$ and using 14 levels of refinement at the three singularities, we get $\mathrm{cap}(\Omega) = 0.496668$ and $\mathrm{cap}(\tilde{\Omega}) = 2.01353$, resulting in error order $= 7$. The map is shown in Figure 6.5e. The corresponding horizontal or u-coordinates of the slits are

$$\{(0.0643908, 0.640592), (0.75947, 0.962074)\}.$$

Interestingly, in the R-type problem the error order decreases only slightly in comparison despite the numerical estimation of the jumps.

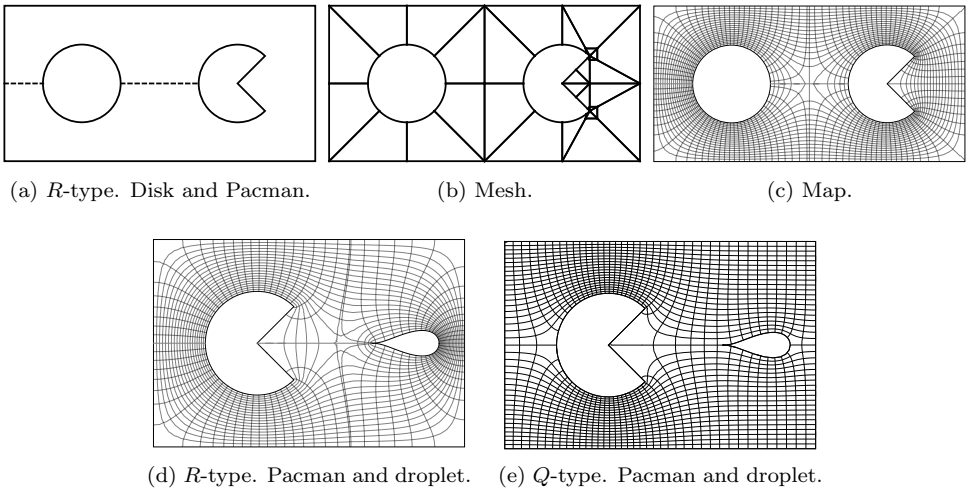

(a) R-type. Disk and Pacman. (b) Mesh. (c) Map.

(d) R-type. Pacman and droplet. (e) Q-type. Pacman and droplet.

FIG. 6.5. *Axially symmetric cases.*

7. Advanced examples. Our last two examples illustrate the versatility of our approach in problems where the cuts have to be computed numerically or the domains are not polycircular-arc.

7.1. *R*-type with multiple regions. Let us consider a case with seven regions, five circles C_i, and two triangles T_j (Figure 7.1) scattered in the unit square. There are six saddle points s_k. The exact locations are given in Table 7.1. In this case also the cuts have to be computed numerically, and thus finding the saddle points is the crucial first step. Once the cuts have been identified, they must be embedded into the conjugate mesh. In contrast with the previous cases, the mesh lines cannot be enforced a priori. In this case we have chosen to approximate the cuts with linear segments rather than curves, which would be more natural in the p-version setting. This is due to maturity of the tools available for constrained triangulation.

Since the geometric complexity is greater, the algorithm naturally does more geometric computations and consequently operates outside the fast kernels, such as linear algebra routines. In this particular case, locating the saddle points took one minute and finding cuts an additional four minutes, in contrast to two minutes spent in integration, which is the typical bottleneck in p-version computations.

The derived results are summarized in Figures 7.1 and 7.2. We get $\mathrm{cap}(\Omega) = 14.2324$ with error order $= 2$. The error order is slightly disappointing, especially in comparison with our other experiments. In addition to errors from geometric approximation, there is also an additional source of error, namely the integration of the jumps when one contour line intersects multiple jumps, since one has to rely on pointwise evaluation of both the potentials and their derivatives. Convergence in capacity does not imply the same pointwise convergence rates. For instance, for the largest region there are four cuts emanating from it. Thus, the resolution of the contour lines is also something one should consider.

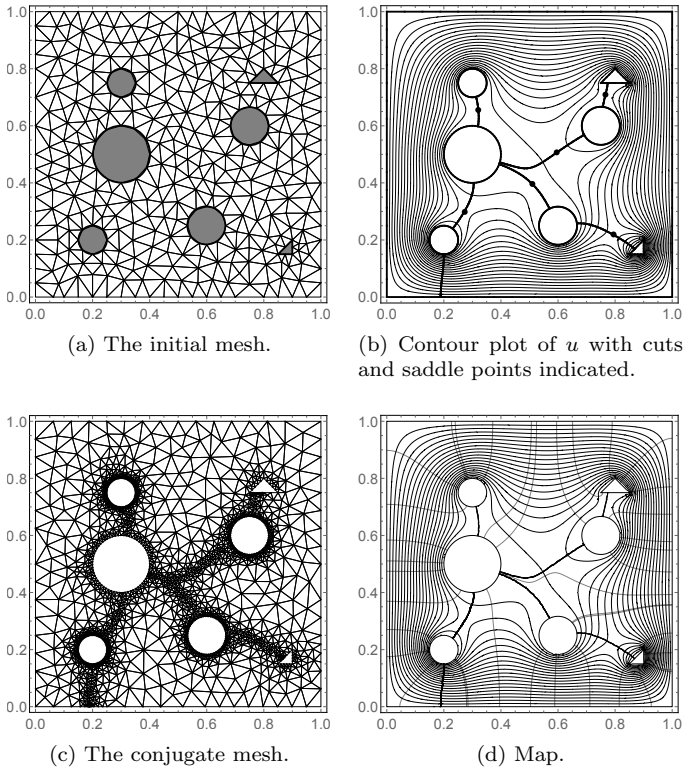

(a) The initial mesh.

(b) Contour plot of u with cuts and saddle points indicated.

(c) The conjugate mesh.

(d) Map.

FIG. 7.1. *R-type. Multiple regions. The boundary of the conjugate mesh can be traced by starting from the bottom and keeping the interior to the left.*

TABLE 7.1

R-type. Multiple regions. There are five circles c_i defined by their centers and radii, two triangles T_j by their corner points (A, B, C), and six saddle points s_k by their locations (x, y).

C	(x, y)	r
c_1	$(0.3, 0.5)$	$1/10$
c_2	$(0.6, 0.25)$	$1/15$
c_3	$(0.75, 0.6)$	$1/15$
c_4	$(0.3, 0.75)$	$1/20$
c_5	$(0.2, 0.2)$	$1/20$

	T_1	T_2
A	$(3/4, 3/4)$	$(17/20, 3/20)$
B	$(17/20, 3/4)$	$(9/10, 3/20)$
C	$(4/5, 4/5)$	$(9/10, 1/5)$

S	(x, y)
s_1	$(0.51, 0.40)$
s_2	$(0.27, 0.29)$
s_3	$(0.32, 0.66)$
s_4	$(0.60, 0.51)$
s_5	$(0.79, 0.22)$
s_6	$(0.77, 0.71)$

7.2. Q-type with nonsymmetric configuration. Let us consider a Q-type problem where the domain B_0 is enclosed by a parametrized curve,

$$\mathbf{r}(t) = \frac{1}{5}(4 + \cos(5t))(\cos(t)\mathbf{i} + \sin(t)\mathbf{j}),$$

with three scaled copies $B_i = \frac{1}{10}\mathbf{r}(t) + b_i$ scattered within it, where the offsets are $b_1 = -(1/10, 1/5)$, $b_2 = (1/20, 2/5)$, $b_3 = (2/5, 1/15)$. The computational domain $\Omega = B_0 \setminus (\cup_{i=1}^{3} B_i)$. The boundary curve $\mathbf{r}(t)$ is divided into four oriented arcs ζ_i with

	1	2	3	4	5	6	7	8	9	10	11	12	13	14
u	$*$	0.90	0.97	0.97	0.93	0.96	0.96	0.93	0.95	0.74	0.74	0.95	0.90	$*$
v	0	0.17	0.23	0.36	0.38	0.40	0.53	0.62	0.62	0.64	0.82	0.93	0.94	1

(a) Data over the cuts. u is the potential at the saddle point; v is the Dirichlet boundary data.

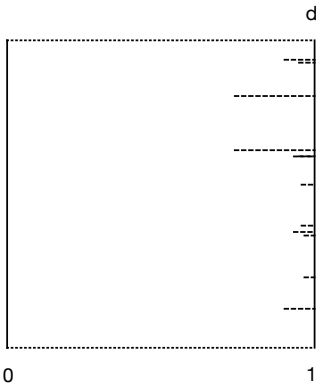

(b) Canonical domain in (u, v). Slit domain scaled to $d = 1$.

FIG. 7.2. *R-type. Multiple regions. Canonical domain and configuration data.*

points

$$q_i = \{(0.997045, 0.0313334), (-0.0241459, 0.768334), \\ (-0.602165, -0.0189238), (0.0261114, -0.830877)\}.$$

So, the problem can be stated as

$$\text{(7.1)} \qquad \begin{cases} \Delta u = 0 & \text{in } \Omega, \\ u = 0 & \text{on } \zeta_1, \\ u = 1 & \text{on } \zeta_3, \end{cases} \qquad \text{leading to} \qquad \begin{cases} \Delta v = 0 & \text{in } \tilde{\Omega}, \\ v = 0 & \text{on } \zeta_2, \quad v = v_1, \quad \text{on } B_1, \\ v = 1 & \text{on } \zeta_4, \quad v = v_2, \quad \text{on } B_2, \\ v = v_3 & \text{on } B_3. \end{cases}$$

The initial mesh is piecewise linear and thus not exact in the sense of the examples above. In Figure 7.3d we let $p = 2, \ldots, 16$ and show the convergence graph of the reciprocal error (loglog). The observed rate is 1.87, indicating algebraic convergence. The initial computed Dirichlet boundary conditions for the conjugate problem are

$$v_1 = 0.403375, \ v_2 = 0.592293, \ v_3 = 0.323098,$$

and after five steps of the interior point method, are corrected to

$$v_1 = 0.501596, \ v_2 = 0.736346, \ v_3 = 0.358485,$$

and the corresponding horizontal or u-coordinates of the slits are

$$\{(0.588018, 0.831274), (0.1605, 0.43309), (0.128553, 0.416906)\}.$$

We get $\text{cap}(\Omega) = 0.908799$, $\text{cap}(\tilde{\Omega}) = 1.101067$, and error order $= 4$. The mesh has 2689 nodes, 7273 edges, and 4582 triangles. In this case, when $p = 4$ the time

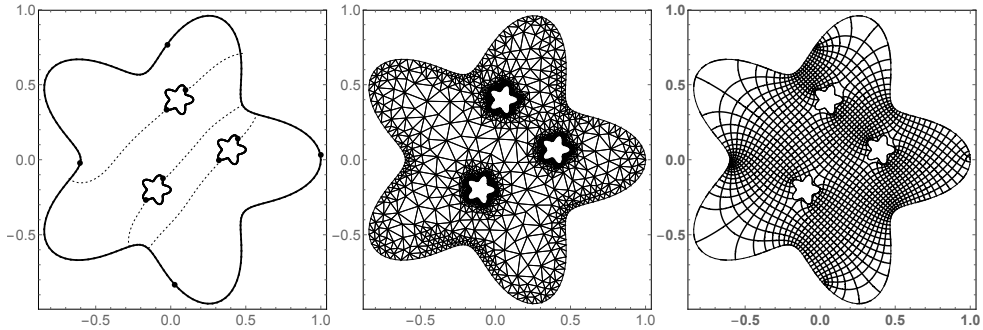

(a) Domain with the four corners of the quadrilateral and the local maxima and minima indicated.

(b) Mesh.

(c) Map.

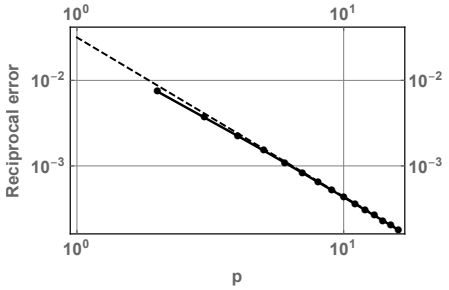

(d) Convergence of the reciprocal error in $p \in [2, 16]$; loglog-plot, rate = 1.87.

FIG. 7.3. *Q-type. Domain enclosed by a parametrized curve* $\mathbf{r}(t) = \frac{1}{5}(4 + \cos(5t))(\cos(t)\mathbf{i} + \sin(t)\mathbf{j})$.

to determine the Dirichlet boundary conditions for the conjugate problem was only four seconds, whereas the integration took 11 seconds, with the initial linear solution taking an additional two seconds, and five steps of the interior point method took 20 seconds.

8. Conclusions. We have introduced algorithms for computation of conformal mappings in multiply connected domains for two specific classes of problems. However, the fundamental ideas can be applied to address a much wider class of problems. Our method relies on numerical solution of PDEs and therefore can be applied to general domains using standard tools with the addition of geometric operations, such as finding paths of steepest descent. In terms of computational cost, the method is competitive, especially in cases where the p-version of FEM can be applied directly. In our current implementation the geometric operations become expensive as the complexity of the configuration increases.

Acknowledgments. The authors wish to thank Professor R. Michael Porter for his careful reading of an earlier version of this manuscript. The authors also wish to thank Professor T. DeLillo and Dr. E. Kropf for help in setting up the example of section 6.1.1. Finally, we wish to thank the anonymous referees, who helped us improve this paper considerably.

REFERENCES

[1] L.V. Ahlfors, *Conformal invariants: Topics in geometric function theory*, McGraw-Hill Book Co., 1973.

[2] L.V. Ahlfors, *Complex Analysis. An Introduction to the Theory of Analytic Functions of One Complex Variable*, 3rd ed., Internat. Ser. Pure Appl. Math., McGraw-Hill Book Co., 1978.

[3] D. Betsakos, K. Samuelsson, and M. Vuorinen, *The computation of capacity of planar condensers*, Publ. Inst. Math. (Beograd) (N.S.), 75(89) (2004), pp. 233–252.

[4] D.G. Crowdy, *The Schwarz-Christoffel mapping to bounded multiply connected polygonal domains*, Proc. R. Soc. Lond. Ser. A Math. Phys. Eng. Sci., 461 (2005), pp. 2653–2678.

[5] D.G. Crowdy, *Schwarz-Christoffel mappings to unbounded multiply connected polygonal regions*, Math. Proc. Cambridge Philos. Soc., 142 (2007), pp. 319–339.

[6] D.G. Crowdy, A.S. Fokas, and C.C. Green, *Conformal mappings to multiply connected polycircular arc domains*, Comput. Methods Funct. Theory, 11 (2012), pp. 685–706.

[7] D.G. Crowdy and C.C. Green, *The Schottky-Klein Prime Function MATLAB Files*, http://www2.imperial.ac.uk/~dgcrowdy/SKPrime, 2010.

[8] D.G. Crowdy and J.S. Marshall, *Computing the Schottky-Klein prime function on the Schottky double of planar domains*, Comput. Methods Funct. Theory, 7 (2007), pp. 293–308.

[9] T.K. DeLillo, A.R. Elcrat, and J.A. Pfaltzgraff, *Schwarz-Christoffel mapping of multiply connected domains*, J. Anal. Math., 94 (2004), pp. 17–47.

[10] T.K. DeLillo, A.R. Elcrat, and E.H. Kropf, *Calculation of resistances for multiply connected domains using Schwarz-Christoffel transformations*, Comput. Methods Funct. Theory, 11 (2012), pp. 725–745.

[11] T.A. Driscoll, *A MATLAB toolbox for Schwarz-Christoffel mapping*, ACM Trans. Math. Software, 22 (1996), pp. 168–186.

[12] T.A. Driscoll, *The Schwarz-Christoffel Toolbox for MATLAB*, http://www.math.udel.edu/~driscoll/SC/, 2009.

[13] T.A. Driscoll and L.N. Trefethen, *Schwarz-Christoffel Mapping*, Cambridge Monogr. Appl. Comput. Math. 8, Cambridge University Press, 2002.

[14] H. Grunsky, *Lectures on Theory of Functions in Multiply Connected Domains*, Vandenhoeck & Ruprecht, 1978.

[15] H. Hakula, T. Quach, and A. Rasila, *Conjugate function method for numerical conformal mappings*, J. Comput. Appl. Math., 237 (2013), pp. 340–353.

[16] H. Hakula, A. Rasila, and M. Vuorinen, *On moduli of rings and quadrilaterals: Algorithms and experiments*, SIAM J. Sci. Comput., 33 (2011), pp. 279–302, https://doi.org/10.1137/090763603.

[17] H. Hakula, A. Rasila, and M. Vuorinen, *Computation of exterior moduli of quadrilaterals*, Electron. Trans. Numer. Anal., 40 (2013), pp. 436–451.

[18] H. Hakula, A. Rasila, and M. Vuorinen, *Conformal modulus and planar domains with strong singularities and cusps*, Electron. Trans. Numer. Anal., 48 (2018), pp. 462–478.

[19] H. Hakula and T. Tuominen, *Mathematica implementation of the high order finite element method applied to eigenproblems*, Computing, 95 (2013), pp. 277–301.

[20] J.A. Iadanza, R. Singh, S.T. Ventrone, and I.L. Wemple, *Method for Designing an Integrated Circuit Having Multiple Voltage Domains*, US Patent 7,000,214, filed November 19, 2003, and issued February 14, 2006.

[21] P. Koebe, *Abhandlungen zur Theorie der konformen Abbildung.* IV. *Abbildung mehrfach zusammenhängender schlichter Bereiche auf Schlitzbereiche*, Acta Math., 41 (1916), pp. 305–344.

[22] O. Lehto and K.I. Virtanen, *Quasiconformal Mappings in the Plane*, Springer, Berlin, 1973.

[23] W. Luo, J. Dai, X. Gu, and S.-T. Yau, *Numerical conformal mapping of multiply connected domains to regions with circular boundaries*, J. Comput. Appl. Math., 233 (2010), pp. 2940–2947.

[24] A. Mayo, *Rapid methods for the conformal mapping of multiply connected regions*, J. Comput. Appl. Math., 14 (1986), pp. 143–153.

[25] Z. Nehari, *Conformal Mapping*, McGraw-Hill Book Co., 1952.

[26] N. Papamichael and N.S. Stylianopoulos, *Numerical Conformal Mapping: Domain Decomposition and the Mapping of Quadrilaterals*, World Scientific, 2010.

[27] L. Reichel, *A fast method for solving certain integral equations of the first kind with application to conformal mapping*, J. Comput. Appl. Math., 14 (1986), pp. 125–142.

[28] O. Séte and J. Liesen, *On conformal maps from multiply connected domains onto lemniscatic domains*, Electron. Trans. Numer. Anal., 45 (2016), pp. 1–15.

[29] L.N. Trefethen, *Numerical computation of the Schwarz–Christoffel transformation*, SIAM J. Sci. Stat. Comput., 1 (1980), pp. 82–102, https://doi.org/10.1137/0901004.
[30] L.N. Trefethen, *Analysis and design of polygonal resistors by conformal mapping*, Z. Angew. Math. Phys., 35 (1984), pp. 692–704.
[31] Wolfram Research, Inc., *Mathematica, Version* 11.3, 2018.
[32] W. Zeng, X. Yin, M. Zhang, F. Luo, and X. Gu, *Generalized Koebe's method for conformal mapping multiply connected domains*, in Proceedings of the 2009 SIAM/ACM Joint Conference on Geometric and Physical Modeling, ACM, 2009, pp. 89–100.